Accepted Manuscript

Nanotubular structures through templateless electropolymerization using thieno[3,4-*b*]thiophene derivatives with different substituents and water content

Omar Sane, Alioune Diouf, Miaobo Pan, Gabriela Morán Cruz, Farah Savina, Rachel Méallet-Renault, Samba Yandé Dieng, Sonia Amigoni, Frédéric Guittard, Thierry Darmanin

PII: S0013-4686(19)31442-2

DOI: https://doi.org/10.1016/j.electacta.2019.134594

Article Number: 134594

Reference: EA 134594

To appear in: *Electrochimica Acta*

Received Date: 12 May 2019

Revised Date: 8 July 2019

Accepted Date: 25 July 2019

Please cite this article as: O. Sane, A. Diouf, M. Pan, Gabriela.Morá. Cruz, F. Savina, R. Méallet-Renault, Samba.Yandé. Dieng, S. Amigoni, Fréé. Guittard, T. Darmanin, Nanotubular structures through templateless electropolymerization using thieno[3,4-*b*]thiophene derivatives with different substituents and water content, *Electrochimica Acta* (2019), doi: https://doi.org/10.1016/j.electacta.2019.134594.

Nanotubular structures through templateless electropolymerization using thieno[3,4-*b*]thiophene derivatives with different substituents and water content

Omar Sane,[a] Alioune Diouf,[a] Miaobo Pan [b], Gabriela Morán Cruz,[b] Farah Savina,[b] Rachel Méallet-Renault,[b] Samba Yandé Dieng,[a] Sonia Amigoni,[c] Frédéric Guittard,[c] Thierry Darmanin[c,*]

[a]*Université Cheikh Anta Diop, Faculté des Sciences et Techniques, Département de Chimie, B.P. 5005 Dakar, Sénégal.*

[b]*University Paris-Sud & Université Paris-Saclay, Institut des Sciences Moléculaires d'Orsay (ISMO), CNRS, F-91405 Orsay, France.*

[c]*Université Côte d'Azur, NICE Lab, IMREDD, 61-63 Av. Simon Veil, 06200 Nice, France.*

Fax: (+33)492076156; Tel: (+33)492076159

E-mail: thierry.darmanin@unice.fr

Abstract

Here, we report a strategy to prepare controllable nanotubular structures using a templateless electropolymerization process in organic solvent (CH_2Cl_2) and without surfactant. We use thieno[3,4-*b*]thiophene derivatives with various substituents including hydrocarbon chains, fluorocarbon chains and aromatic groups of various size. The influence of the water content (CH_2Cl_2 + H_2O) in also studied in order to release *in-situ* a higher amount of gas bubbles (O_2 and/or H_2). The best results are obtained with the pyrene substituent, which lead to highly densely packed nanotubular structures while the water content allows to highly increase their porosity, changing the resulting surface morphology from tree-like to coral-like structure. This is probably due to both high π-stacking interaction of pyrene and its polymerization capacity in the same potential range. This change also induces an increase in surface hydrophilicity because the water highly penetrates these porous structures. Moreover, both the poly(thieno[3,4-b]thiophene) polymers and the substituents participate to the film

fluorescence while the nanostructures seem to amplify their intensity. Such surfaces are extremely interesting for potential applications in sensors or in water harvesting systems.

Keywords: Nanostructures, Nanotubes, Wettability, Hydrophobicity, Conducting polymers.

1. Introduction

The design of nanoporous surfaces such as nanotubes with well-controlled dimensions (diameter, height, porosity) and shape are fundamental to understand well the relationship between geometrical parameters of the nanostructures and the surface properties [1]. The range of possible applications of these nanoporous surfaces is extremely large [2-7]. For example, nanotubular surfaces were employed to encapsulate both molecules, materials and even gases and various applications are expected such as in drug delivery, biomedical imaging, while nanocomposites could also be used in catalysis, electrocatalysis, photocatalysis, batteries, supercapacitors, photovoltaics and sensors. The formation of porous structures such as nanotubes is also extremely interesting to control the surface hydrophobicity and water adhesion [8-10]. The air trapped within these nanotubes can indeed affect the surface wettability, as explained in the Cassie-Baxter equation [11-14].

One of the most employed method to produce ordered nanostructures is the use of membranes such as anodized aluminum oxide (AAO) membranes [15-17]. With these membranes, it is possible for example to prepare ordered vertically aligned nanotubes. However, this process is difficult and long to perform. Moreover for each change in the nanotube parameter it is necessary to use another membrane.

The templateless electropolymerization approach is an excellent alternative to produce very quickly porous ordered nanostructures such as nanotubes or nanocups. The pyrrole electropolymerization directly in water (H_2O) was intensively studied in the literature [18-28]. In this process, different gases (O_2 and/or H_2) responsible of the porosity of the nanostructures are produced. A surfactant is used to stabilize the gas bubbles during the polymer growth. Moreover, most of the monomers are not soluble in water while the electropolymerization in water often needs high monomer concentration.

Very recently, it was reported the possibility to obtain very ordered nanoporous structures such as vertically aligned nanotubes using a template-less electropolymerization approach but in organic solvent such as dichloromethane (CH_2Cl_2) and without surfactant [29-36].

Here, trace of water (H_2O) present in solution seemed to be responsible of the formation of gas bubbles (O_2 and/or H_2) directly during the electropolymerization and as a consequence the formation of ordered porous structures. Because no surfactant was used, the used monomer plays a huge role by stabilizing the gas bubbles and allowing the polymer to grow around them. For example, monomers derived from 3,4-phenylenedioxythiophene (PheDOT), 3,4-naphtalenedioxythiophene (NaphDOT) and thienothiophene were found to be excellent candidates. Moreover, it seems that the rigidity of the polymer is a key parameter. It was also possible to obtain parahydrophobic properties with extremely high water apparent contact angle (θ_w) and strong water adhesion [29,30].

In the light of these previous results, we wanted to investigate original thieno[3,4-*b*]thiophene derivatives but using substituent differing by their nature, length and rigidity. The thieno[3,4-b]thiophene core was also selected for their exceptional polymerization capacity and unique opto-electronic properties [37-40]. The studied monomers are represented in Scheme 1. We also report the results obtained with Thieno-OH for comparison. Moreover, we investigate the influence of the water content by saturating the solvent (CH_2Cl_2) with H_2O. For that, we report the results (morphology, hydrophobicity, water adhesion) with anhydrous CH_2Cl_2 and the mixture called CH_2Cl_2 + H_2O. For the first time fluorescence properties of these thienothiophene (here, thieno[3,4-*b*]thiophene) derivatives are also presented.

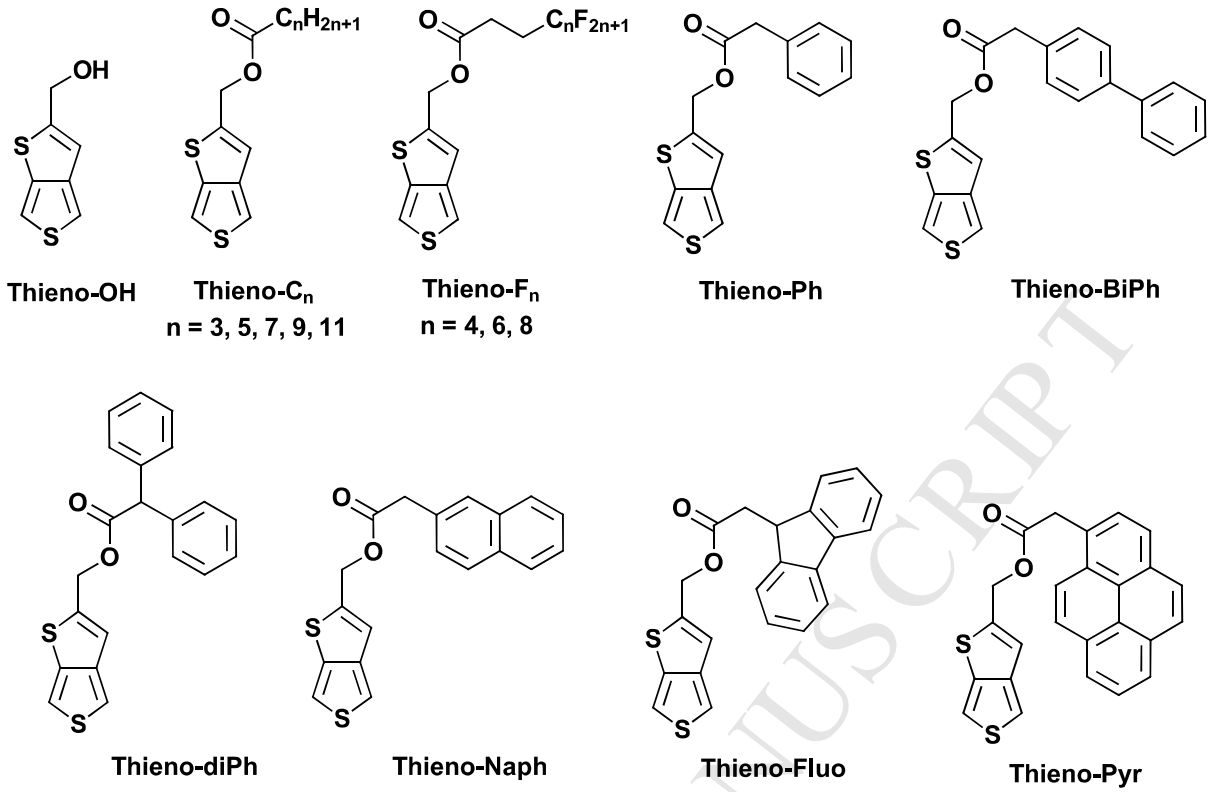

Scheme 1. Monomers studied in this manuscript.

2. Experimental Section

Thieno[3,4-*b*]thiophen-2-ylmethanol (Thieno-OH) was synthesized in three steps from 3,4-dibromothiophene, following a procedure already reported in the literature [40-42].

Thieno-OH: thieno[3,4-*b*]thiophen-2-ylmethanol

Yield 91%; Crystalline solid; m.p 89°C; δ_H(400 MHz, $CDCl_3$): 7.19 (d, J = 2.8 Hz, 1H), 7.13 (d, J = 2.2 Hz, 1H), 6.76 (s, 1H), 4.70 (s, 2H), 1.82 (s, 1H); δ_C(400 MHz, $CDCl_3$): 150.75, 146.73, 138.75, 114.29, 112.01, 110.86, 61.51; GC/MS: 170 ($M^{+\cdot}$, 81), 153 ($C_7H_5OS_2^{+\cdot}$, 100).

Then, the substituted monomers were synthesized by simple esterification reaction at room temperature (Scheme 2). More precisely, 1.2 eq. of the corresponding carboxylic acid, 1.2 eq. 130 g of *N*-(3-dimethylaminopropyl)-*N*′-ethylcarbodiimide hydrochloride (130 mg) and 4-(dimethylamino)pyridine (DMAP) (20 mg) were added to 20 mL of absolute dichloromethane. After stirring for 30 min, 100 mg of Thieno-OH (1eq.) was added to the mixture. After one day, the crude product was purified by column chromatography.

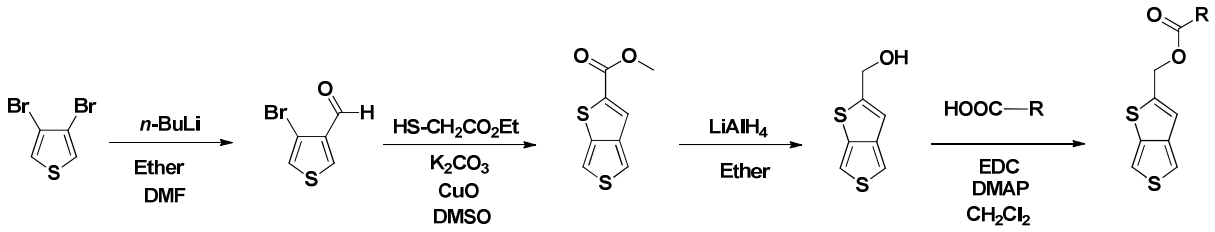

Scheme 2. Chemical way to the monomers.

Thieno-C_3: thieno[3,4-*b*]thiophen-2-ylmethyl butyrate

Yield 49.6%;Crystalline solid; m.p 32°C;δ_H(400 MHz, $CDCl_3$): 7.30 (d, J = 2.6Hz, 1H), 7.20 (d, *J* = 2.3 Hz, 1H), 6.91 (s, 1H), 5.21 (s, 2H), 2.35 (t, J = 7.4Hz, 2H), 1.68(m, 2H), 0.96 (t, J = 7.4Hz, 3H);δ_C(400 MHz, $CDCl_3$): 172.20, 145.38, 143.99, 138.08, 115.99, 111.60, 109.82, 60.80, 35.03, 17.37, 12.64; GC/MS: 240 ($M^{+\cdot}$, 35), 170 ($C_7H_6OS_2^+$, 100), 153 ($C_7H_5S_2^+$, 72)

Thieno-C_5: thieno[3,4-*b*]thiophen-2-ylmethyl hexanoate

Yield 80.8%; Crystalline solid; m.p 49°C; δ_H(400 MHz, $CDCl_3$): 7.30 (d, J = 2.7Hz, 1H), 7.20 (d, *J* = 2.0 Hz, 1H), 6.91 (s, 1H), 5.20 (s, 2H), 2.36 (t, J = 7.5Hz, 2H), 1.65(m, 2H), 1.31(m, 4H), 0.89 (t, J = 6.9Hz, 3H); δ_C(400 MHz, $CDCl_3$): 173.37, 146.37, 144.98, 139.07, 116.98, 112.59, 110.81, 61.81, 34.12, 31.23, 24.54, 22.26, 13.86; GC/MS: 268 ($M^{+\cdot}$, 35), 170 ($C_7H_6OS_2^+$, 100), 153 ($C_7H_5S_2^+$, 60)

Thieno-C_7: thieno[3,4-*b*]thiophen-2-ylmethyl octanoate

Yield 90.4%; Crystalline solid;m.p 58°C; δ_H(400 MHz, $CDCl_3$): 7.30 (d, J = 2.6Hz, 1H), 7.20 (d, *J* = 2.3 Hz, 1H), 6.91 (s, 1H),5.20 (s, 2H),2.36 (t, J = 7.5Hz, 2H),1.64 (m, 2H), 1.28 (m, 8H), 0.88 (t, J = 6.8Hz, 3H); δ_C(400 MHz, $CDCl_3$): 172.40, 145.39, 143.99, 138.09, 116.01, 111.60, 109.81, 60.81, 33.19, 30.61, 28.03, 27.87, 23.88, 21.55, 13.04; GC/MS: 296 ($M^{+\cdot}$, 44), 170 ($C_7H_6OS_2^+$, 100), 153 ($C_7H_5S_2^+$, 60)

Thieno-C_9: thieno[3,4-*b*]thiophen-2-ylmethyl decanoate

Yield 83.7%; Crystalline solid; m.p 68°C; δ_H(400 MHz, $CDCl_3$): 7.30 (d, J = 2.6Hz, 1H), 7.20 (d, *J* = 2.1 Hz, 1H), 6.91 (s, 1H),5.20 (s, 2H), 2.36 (t, J = 7.5Hz, 2H), 1.64(m, 2H), 1.27(m, 12H), 0.88 (t, J = 6.2Hz, 3H); δ_C(400 MHz, $CDCl_3$): 173.39, 146.38, 144.99, 139.08, 116.99, 112.59, 110.80, 61.81, 34.17, 31.82, 29.37, 29.21, 29.08, 24.87, 22.63, 14.09; GC/MS: 324 ($M^{+\cdot}$, 45), 170 ($C_7H_6OS_2^+$, 100), 153 ($C_7H_5S_2^+$, 61)

Thieno-C_{11}: thieno[3,4-*b*]thiophen-2-ylmethyl dodecanoate

Yield 66.4%; Crystalline solid; m.p 78°C; δ_H(400 MHz, $CDCl_3$): 7.30 (d, J = 2.6Hz, 1H), 7.20 (d, *J* = 2.6 Hz, 1H), 6.91 (s, 1H), 5.20 (s, 2H), 2.36 (t, J = 7.5Hz, 2H), 1.64(m, 2H), 1.27(m, 16H), 0.88 (t, J = 6.8Hz, 3H); δ_C(400 MHz, $CDCl_3$): 173.40, 146.39, 145.00, 139.09, 116.99,

112.60, 110.81, 61.81, 34.18, 31.89, 29.58, 29.42, 29.31, 29.22, 29.09, 24.88, 22.67, 14.10; GC/MS: 352 ($M^{+\cdot}$, 42), 170 ($C_7H_6OS_2^+$, 100), 153 ($C_7H_5S_2^+$, 61)

Thieno-F_4: thieno[3,4-*b*]thiophen-2-ylmethyl 4,4,5,5,6,6,7,7,7-nonafluoroheptanoate

Yield 60.4%; Crystalline solid; m.p 55°C; δ_H(400 MHz, $CDCl_3$):7.27 (d, J = 2.5Hz, 1H),7.15 (d, *J* = 2.6 Hz, 1H),6.86 (s, 1H),5.18(s, 2H), 2.63 (t, J = 7.3Hz, 2H), 2.42(tt, J = 18.2Hz, J = 8.2Hz, 2H); δ_C(400 MHz, $CDCl_3$): 170.70, 146.22, 143.97, 138.98, 117.62, 112.99, 111.01, 62.68, 26.35, 25.42; δ_F(200 MHz, $CDCl_3$): -81.04, -115.03, -124.48, -126.07; GC/MS: 444 ($M^{+\cdot}$, 50), 170 ($C_7H_6OS_2^+$, 100), 153 ($C_7H_5S_2^+$, 44)

Thieno-F_6: thieno[3,4-*b*]thiophen-2-ylmethyl 4,4,5,5,6,6,7,7,8,8,9,9,9-tridecafluorononanoate

Yield 52.3%; Crystalline solid; m.p 73°C; δ_H(400 MHz, $CDCl_3$): 7.33 (d, J = 2.6Hz, 1H), 7.22 (d, *J* = 2.6 Hz, 1H), 6.94 (s, 1H), 5.26 (s, 2H), 2.70 (t, J = 7.3Hz, 2H), 2.50 (tt, J = 18.2Hz, J = 8.2Hz, 2H); δ_C(400 MHz, $CDCl_3$): 170.70, 146.22, 143.97, 138.98, 117.62, 112.99, 111.01, 62.68, 26.45, 25.45;δ_F(200 MHz, $CDCl_3$): -80.81, -114.80, -121.94, -122.91, -123.52, -126.18; GC/MS: 544 ($M^{+\cdot}$, 33), 170 ($C_7H_6OS_2^+$, 100), 153 ($C_7H_5S_2^+$, 37)

Thieno-F_8: thieno[3,4-*b*]thiophen-2-ylmethyl4,4,5,5,6,6,7,7,8,8,9,9,10,10,11,11,11heptadecafluoroundecanoate

Yield 70.0%; Crystalline solid; m.p 91°C; δ_H(400 MHz, $CDCl_3$): 7.33 (d, J = 2.7Hz, 1H),7.23 (d, *J* = 2.7 Hz, 1H),6.94 (s, 1H),5.25 (s, 2H), 2.70 (t, J = 7.3Hz, 2H), 2.50 (tt, J = 18.1Hz, J = 8.4, 2H); δ_C(400 MHz, $CDCl_3$):170.72, 146.23, 143.98, 138.99, 117.62, 112.99, 111.00, 62.68, 26.46, 25.43;δ_F(200 MHz, $CDCl_3$): -80.78, -114.78, -121.87, -122.73, -123.49, -126.18 GC/MS: 643.9 ($M^{+\cdot}$, 30), 170 ($C_7H_6OS_2^+$, 100), 153 ($C_7H_5S_2^+$, 25)

Thieno-Ph: thieno[3,4-*b*]thiophen-2-ylmethyl 2-(cyclohexa-1,5-dien-1-yl)acetate

Yield 87%; Crystalline solid; m.p 59°C; δ_H(400 MHz, $CDCl_3$): 7.31 (m, 5H), 7.29 (d, J = 1.8Hz, 1H), 7.21 (d, *J* = 2.1 Hz, 1H), 6.89 (s, 1H), 5.22(s, 2H), 3.69 (s, 2H); δ_C(400 MHz, $CDCl_3$): 171.12, 146.34, 144.57, 139.06, 133.56, 129.48, 129.32, 128.70, 128.60, 127.20, 117.15, 112.69, 110.85, 62.41, 41.15; GC/MS: 288 ($M^{+\cdot}$, 55), 170 ($C_7H_6OS_2^+$, 80), 153 ($C_7H_5S_2^+$, 100)

Thieno-BiPh: thieno[3,4-*b*]thiophen-2-ylmethyl 2-([1,1'-biphenyl]-4-yl)acetate

Yield 66.4%; Crystalline solid; m.p 126°C; δ_H(400 MHz, $CDCl_3$): 7.54 (m, 5H), 7.42 (t, 2H), 7.38 (m, 2H), 7.31 (d, J = 2.7Hz, 1H), 7.21 (d, *J* = 2.7 Hz, 1H), 6.90 (s, 1H), 5.25 (s, 2H), 3.73 (s, 2H); δ_C(400 MHz, $CDCl_3$): 171.11, 146.33, 144.53, 140.74, 140.18, 139.06, 132.94,

132.57, 129.92, 129.74, 128.74, 127.45, 127.35, 127.28, 127.06, 117.23, 112.73, 110.87, 62.48, 48.81, 40.78; GC/MS: 240 ($M^{+\cdot}$, 35), 170 ($C_7H_6OS_2^+$, 100), 153 ($C_7H_5S_2^+$, 25).

Thieno-diPh: thieno[3,4-*b*]thiophen-2-ylmethyl 2-(cyclohexa-1,5-dien-1-yl)-2-phenylacetate

Yield 64.5%; Crystalline solid; m.p 131°C; δ_H(400 MHz, $CDCl_3$): 7.31 (d, J = 4.3Hz, 6H), 7.29 (d, J = 2.0Hz, 2H), 7.28 (d, *J* = 1.9 Hz, 2H), 6.86 (s, 1H), 5.27(s, 2H), 5.09 (s, 1H); δ_C(400 MHz, $CDCl_3$): 172.08, 146.31, 144.39, 138.29, 136.84, 128.74, 128.67, 128.61, 127.62, 127.33, 117.27, 112.68, 110.82, 62.69, 56.92.

Thieno-Naph: thieno[3,4-*b*]thiophen-2-ylmethyl 2-(naphthalen-1-yl)acetate

Yield 90.9%; Crystalline solid; m.p 124°C; δ_H(400 MHz, $CDCl_3$): 7.30 (d, J = 2.6Hz, 1H), 7.20 (d, *J* = 2.6 Hz, 1H), 6.91 (s, 1H), 5.20 (s, 2H), 2.36 (t, J = 7.5Hz, 2H), 1.64(m, 2H), 1.27(m, 16H), 0.88 (t, J = 6.8Hz, 3H); δ_C(400 MHz, $CDCl_3$): 173.40, 146.39, 145.00, 139.09, 116.99, 112.60, 110.81, 61.81, 34.18, 31.89, 29.58, 29.42, 29.31, 29.22, 29.09, 24.88, 22.67, 14.10; Mass: GC/MS: 240 ($M^{+\cdot}$, 35), 170 ($C_7H_6OS_2^+$, 100); 153 ($C_7H_5S_2^+$, 25).

Thieno-Fluo: thieno[3,4-*b*]thiophen-2-ylmethyl 2-(9H-fluoren-9-yl)acetate

Yield 63.9%; Crystalline solid; m.p 79°C; δ_H(400 MHz, $CDCl_3$): 7.65 (d, J = 7.6Hz, 2H), 7.39 (d, *J* = 7.5Hz, 2H), 7.28 (t, J = 7.5Hz, 3H), 7.25 (d, J = 2.7Hz, 1H), 7.18 (m, 1H), 7.16 (m, 1H), 7.14 (d, J = 2.7Hz, 1H), 6.86 (s, 1H), 5.24 (s, 2H), 4.36 (t, J = 7.1Hz, 1H), 2.77 (d, J = 7.2Hz, 2H),; δ_C(400 MHz, $CDCl_3$): 172.04, 146.34, 146.00, 144.41, 140.74, 139.10, 127.48, 127.16, 124.36, 119.92, 117.53, 112.80, 110.89, 65.84, 62.22, 43.50, 38.48; Mass: GC/MS: 240 ($M^{+\cdot}$, 35), 170 ($C_7H_6OS_2^+$, 100).

Thieno-Pyr: thieno[3,4-*b*]thiophen-2-ylmethyl 2-(pyren-1-yl)acetate

Yield 99%; Crystalline solid; m.p 93°C; δ_H(400 MHz, $CDCl_3$): 8.09 (m, 9H), 7.23 (d, *J* = 2.6 Hz, 1H), 7.18 (d, *J* = 2.3 Hz, 1H), 6.81 (s, 1H), 5.23 (s, 2H), 4.41 (s, 2H); δ_C(400 MHz, $CDCl_3$): 171.15, 146.31, 144.47, 139.05, 131.27, 130.90, 130.76, 129.46, 128.41, 127.98, 127.98, 127.62, 127.38, 127.33, 125.97, 125.27, 125.15, 125.01, 124.86, 123.16, 117.22, 112.66, 110.80, 62.52, 39.36.

Electropolymerization parameters

The templateless electropolymerization experiments were performed with an Autolab potentiostat of Metrohm (Autolab). A three-electrode system was used with a 2 cm^2 gold plates as working electrode (or ITO slide for luminescence experiment), a carbon rod as counter-electrode and a saturated calomel electrode (SCE) as reference electrode. The working electrodes were purchased from Neyco. Then, 10 mL of the solution was inserted in

an electrochemical cell and connected to the potentiostat thanks to the electrodes. This solution contained 0.1 M of tetrabutylammonium perchlorate (Bu_4NClO_4) as supporting electrolyte and 0.01 M of monomer. The solvent used here was either anhydrous dichloromethane (CH_2Cl_2) or dichloromethane saturated with water, called here CH_2Cl_2 + H_2O. For the preparation of CH_2Cl_2 + H_2O solution, CH_2Cl_2 was mixed with a high amount of H_2O. Then, the excess of H_2O was removed by extraction after decantation. Here, H_2O was added to anhydrous CH_2Cl_2 in order to release a high amount of O_2 and H_2 bubbles. Then, the electrodepositions were performed by cyclic voltammetry from -1 V to the monomer oxidation potential (here, $E^{ox} \approx 1.75$ V vs SCE) and at a scan rate of 20 mV s^{-1}. Different number of scans were performed (1, 3 and 5) in order to better investigate the polymer growth.

Surface characterization

The morphology was evaluated by the scanning electron microscopy (SEM) with a 6700F microscope of JEOL. For the surface hydrophobicity, a DSA30 goniometer of Bruker was used. 2 µL water droplets were placed on the surface to determine the water apparent contact angles (θ_w) at the triple point. For the dynamic contact angles, the tilted-drop method was used using 6 µL water droplets placed on the surface. Then, the surface was inclined until the droplet moves. The advanced and receding contact angle and as a consequence the hysteresis were taken just before the droplet moves. If the droplet does not move whatever the surface inclination, the surface is called sticky.

UV-vis and Fluorescence steady-state spectroscopy on monomers

The UV-vis absorbance of the monomers was performed using a Shimadzu UV-VIS Spectrophotometer UV-2600, with medium scan speed and 1.0 nm band-pass slits. All the monomers were studied in spectroscopic grade and degassed acetonitrile at a concentration around 10^{-5}mol/L. The emission spectra were recorded on a Fluoromax-4+ Horiba spectrofluorimeter. Excitation wavelength was fixed at 300nm, except for Thieno-Fluo where excitation wavelengths were set at 266nm. Slits size were adjusted in order to get the best signal to noise ratio with avoiding saturation of the detector.

Fluorescence microscopy on films

Fluorescence images were acquired using Leica TCS SP5-AOBS confocal laser scanning microscope. The surfaces were submerged in distilled water, and imaged using × 63- 1.4 numerical aperture plan apochromat oil immersion objective. The size of the *xy* image was 512 × 512 pixels (image sizes: 49.21 × 49.21 µm² and 24.60 × 24.60 µm²) recorded on 12 bits. Films were excited at 476 nm or 488 nm and the emission was collected from 500 to 640 nm or 520-660nm. Laser power was set around 30% and gain was adjusted in order to get signal. Each image corresponds to an average of 3 frames.

3. Results and Discussion

Templateless electropolymerization

The monomer oxidation potential of these two monomers was found to be relatively close ($E^{ox} \approx 1.75$ V vs SCE), independently of the solvent (CH_2Cl_2 or $CH_2Cl_2 + H_2O$). Then, the polymers were electrodeposited by cyclic voltammetry using a scan rate of 20 mV s^{-1} and using different number of scans (1, 3 and 5). Cyclic voltammograms are given in Figure 1 and ESI using the two solvents (CH_2Cl_2 or $CH_2Cl_2 + H_2O$). Here, the influence of H_2O is difficult to see because the intensity of the peaks of re-reduction of oxidized polymers is very important and on a large potential range [35]. For example, in the case of Thieno-OH and following previous results, the following reactions are present using the solvent $CH_2Cl_2 + H_2O$:

- during the forward scans:

$$n\ \text{Thieno-OH} \rightarrow \text{poly(Thieno-OH)}_{reduced} + 2n\ H^+ + 2n\ e^-$$

$$\text{poly(Thieno-OH)}_{reduced} \rightarrow \text{poly(Thieno-OH)}_{oxidized} + m\ e^-$$

$$2\ H_2O \rightarrow \mathbf{O_2}\ (\text{bubbles}) + 4\ H^+ + 4\ e^-$$

- during the back scans:

$$\text{poly(Thieno-OH)}_{oxidized} + m\ e^- \rightarrow \text{poly(Thieno-OH)}_{reduced}$$

$$2\ H_2O + 2\ e^- \rightarrow \mathbf{H_2}\ (\text{bubbles}) + 2\ OH^-$$

With some of the aromatic substituent such as pyrene, it's even more difficult because the substituent can also be oxidized and participate to the polymerization. Indeed their oxidation potential can be in the same range than that of thieno[3,4-*b*]thiophene moiety.

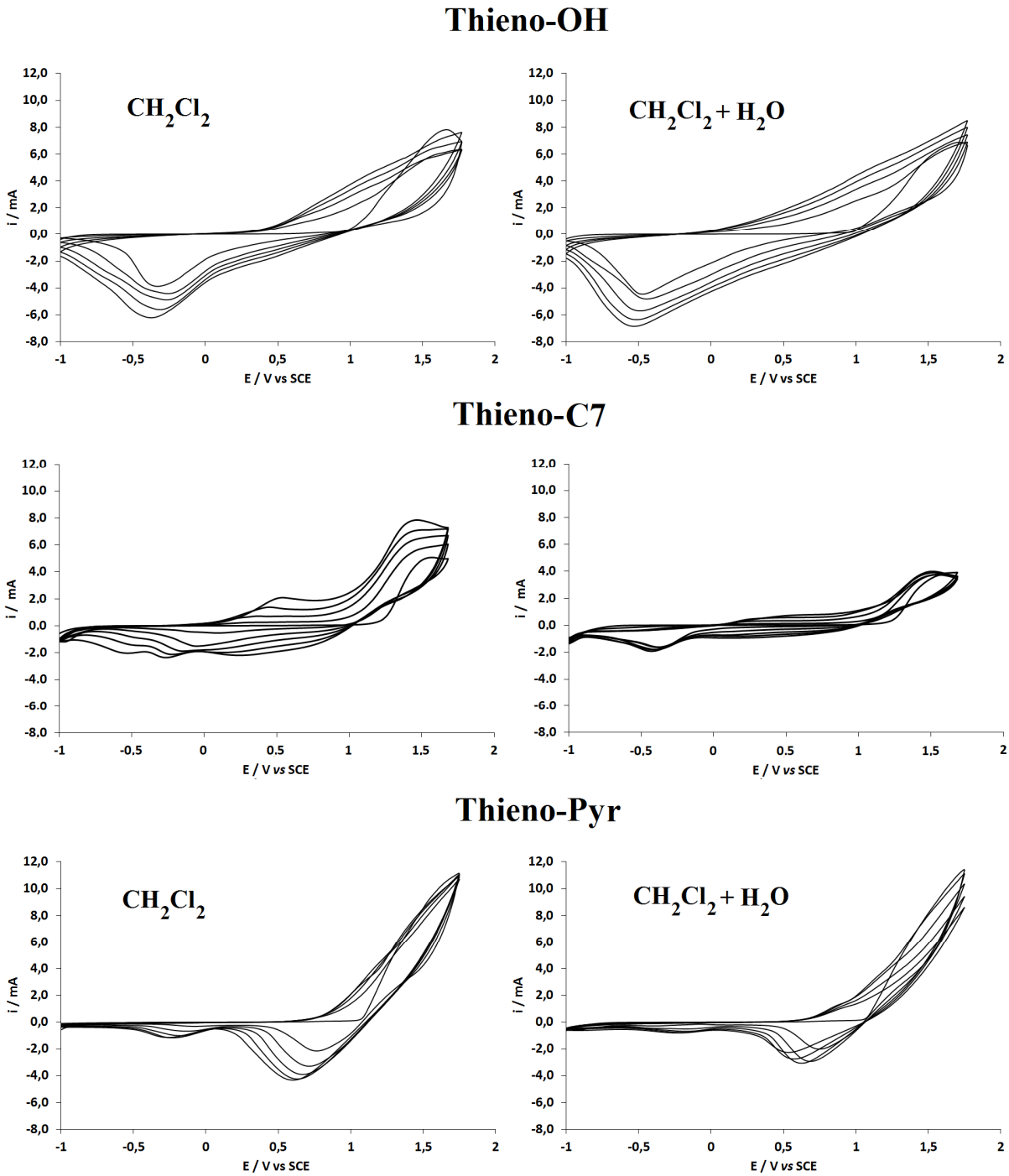

Figure 1. Example of cyclic voltammograms of Thieno-OH, Thieno-C7 and Thieno-Pyr (0.01 M) in anhydrous CH_2Cl_2 or CH_2Cl_2 saturated with water (CH_2Cl_2 + H_2O) with Bu_4NClO_4 (0.1 M); scan rate: 20 mV s^{-1}.

To better estimate the influence of H_2O, cyclic voltammograms were performed in CH_2Cl_2 or CH_2Cl_2 + H_2O without monomer (Figure 2). First of all, a huge peak a ≈ -0.5 V *vs* SCE in well present during the back scan and only in CH_2Cl_2 + H_2O confirming the reaction 2 H_2O + 2 e^- → **H_2** (bubbles) + 2 OH^-. The peak starts at ≈ -0.0 V and go to ≈ -0.85 V. For the reaction

2 $H_2O \rightarrow$ **O_2** (bubbles) + 4 H^+ + 4 e^-, a peak is well present during the forward scan but rather from ≈ 2.0 V *vs* SCE. Hence, in the potential range used here, it is especially expected the formation of H_2 bubbles.

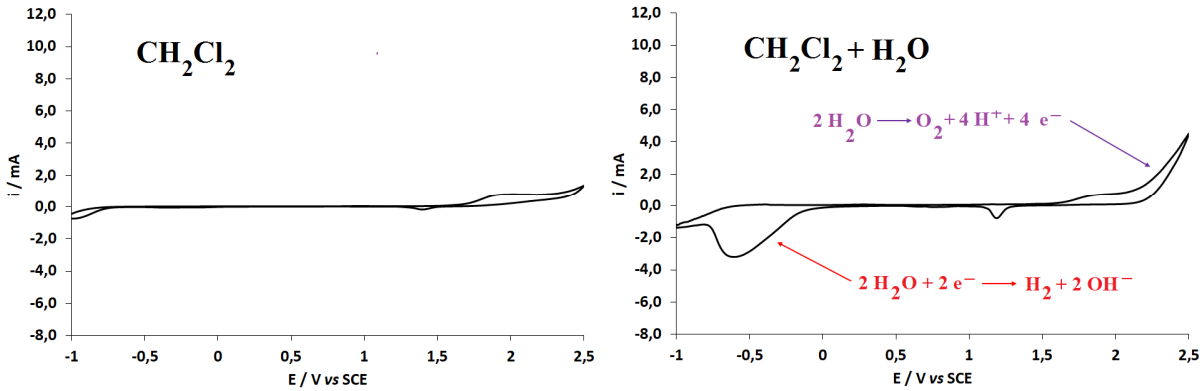

Figure 2. Cyclic voltammograms of CH_2Cl_2 or CH_2Cl_2 + H_2O with Bu_4NClO_4 (0.1 M); scan rate: 20 mV s^{-1}.

To better visualize the presence of the conducting polymers, cyclic voltammograms were performed in CH_2Cl_2 or CH_2Cl_2 + H_2O without monomer and using polymer-coated gold substrates (Figure 3 and ESI). The intensity of the peak is very different depending on the used monomer. It was often observed the presence of one oxidation peak during the forward scans and one reduction peak during the back scans. With some of the monomers, two peaks are observed which should be due to multiple oxidation steps.

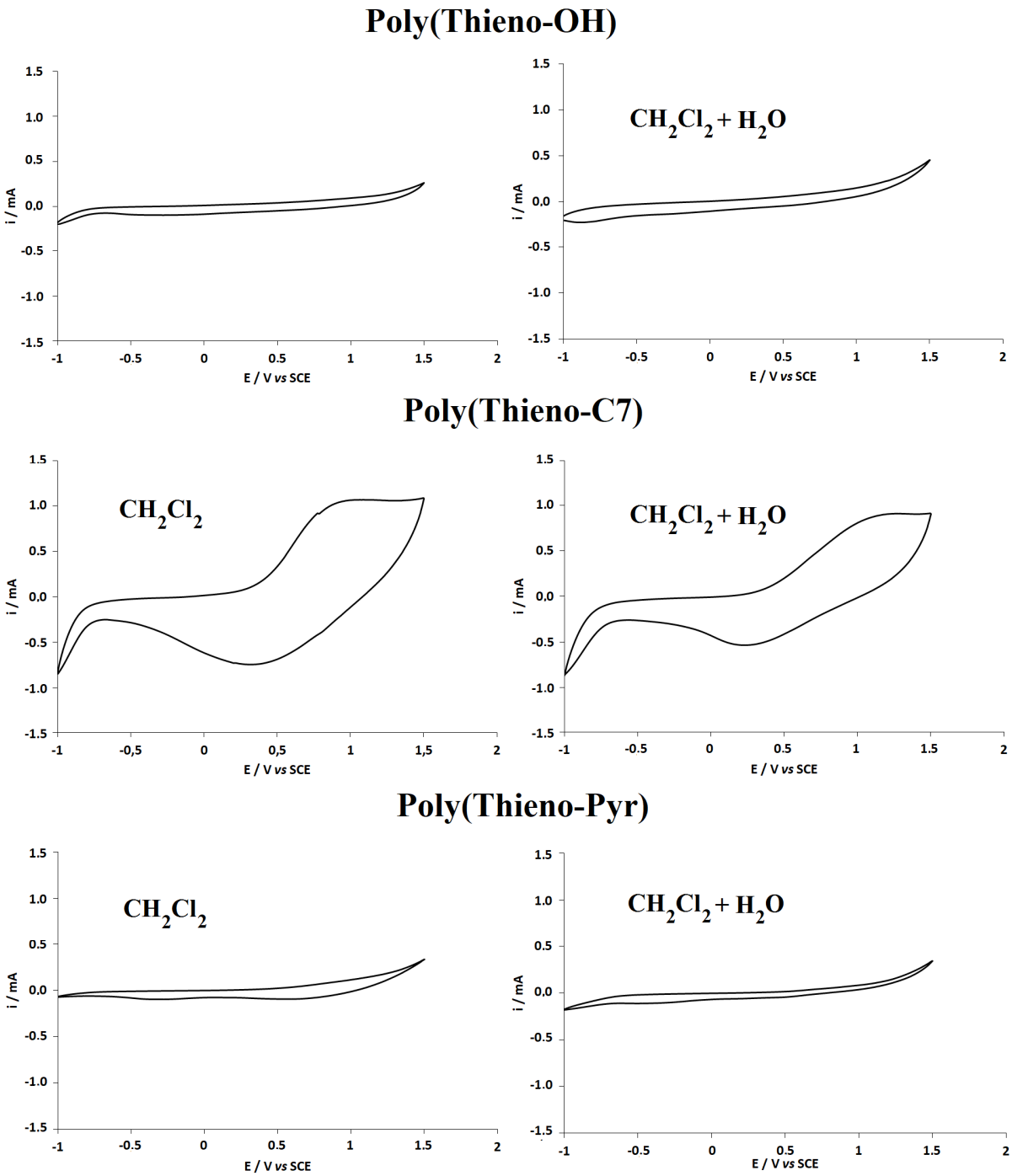

Figure 3. Example of cyclic voltammograms of Poly(Thieno-OH), Poly(Thieno-C7) and Poly(Thieno-Pyr)-coated gold substrates in anhydrous CH_2Cl_2 or CH_2Cl_2 + H_2O with Bu_4NClO_4 (0.1 M); scan rate: 20 mV s^{-1}.

Surface morphology and wettability

Hence, to better visualize the influence of the H_2O, it is necessary to investigate the surface morphology. The surface morphology was investigated by scanning electron microscopy (SEM). The most important observation is that a drastic change in the surface morphology is observed after adding H_2O. This is likely to be due to the formation of a high amount a gas bubbles (O_2 and H_2). Indeed, using anhydrous CH_2Cl_2, the surfaces are extremely rough but almost no porous structures are observed. In opposite, using CH_2Cl_2 + H_2O, a huge amount of porous structures (in particular, hollow spheres) are present on the surface.

Using Thieno-OH, the surfaces are extremely rough and the adding of H_2O leads to a huge amount of porous structures mainly hollow spherical structures (Figure 4). With the monomers substituted by an alkyl chain (Thieno-Cn), it was observed a decrease of the surface roughness as the alkyl chain length increases (Figure 5). The adding of H_2O leads to a huge amount of hollow spherical structures but only with very short alkyl chain (Thieno-C4). This is in opposite to the results obtained with the fluoroalkyl chains (Thieno-Fn) (Figure 6). Here, a high amount of hollow spherical structures is observed with Thieno-F8, which are also all open. Hence, it seems that the rigidity of the polymer is very important to stabilize the gas bubbles during the electropolymerization. The alkyl decreases the rigidity of the polymer because these chains are flexible which is not the case of the fluorinated chains because these chains are known to be rigid, especially long perfluoroalkyl chains.

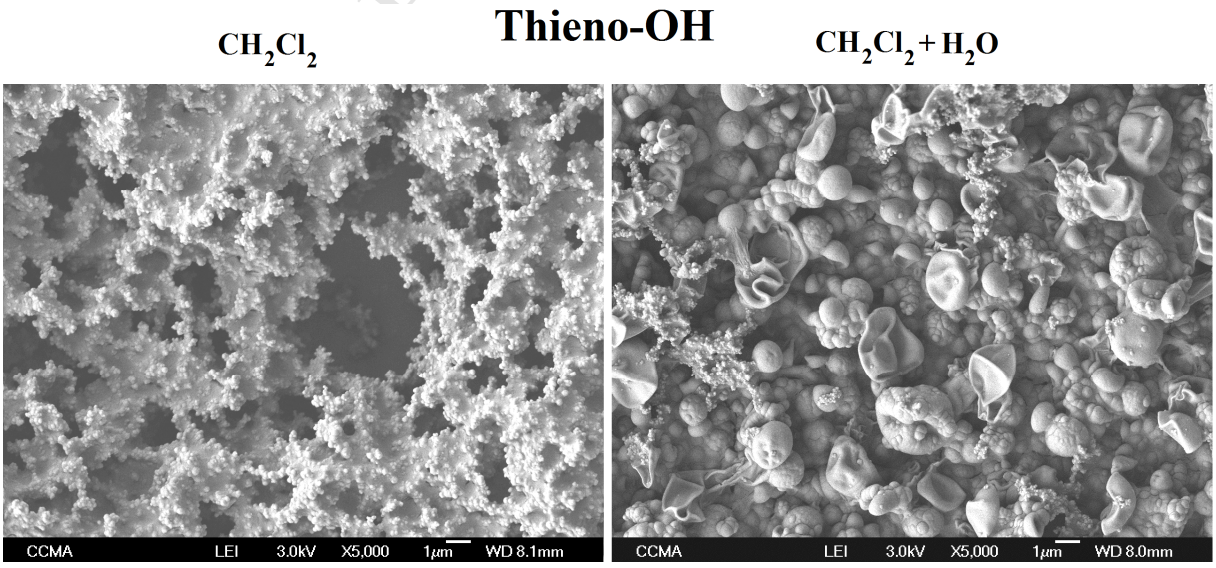

Figure 4. SEM pictures of surfaces obtained from Thieno-OH and using two different electropolymerization solvents (CH_2Cl_2 and CH_2Cl_2 + H_2O). Number of scans: 3.

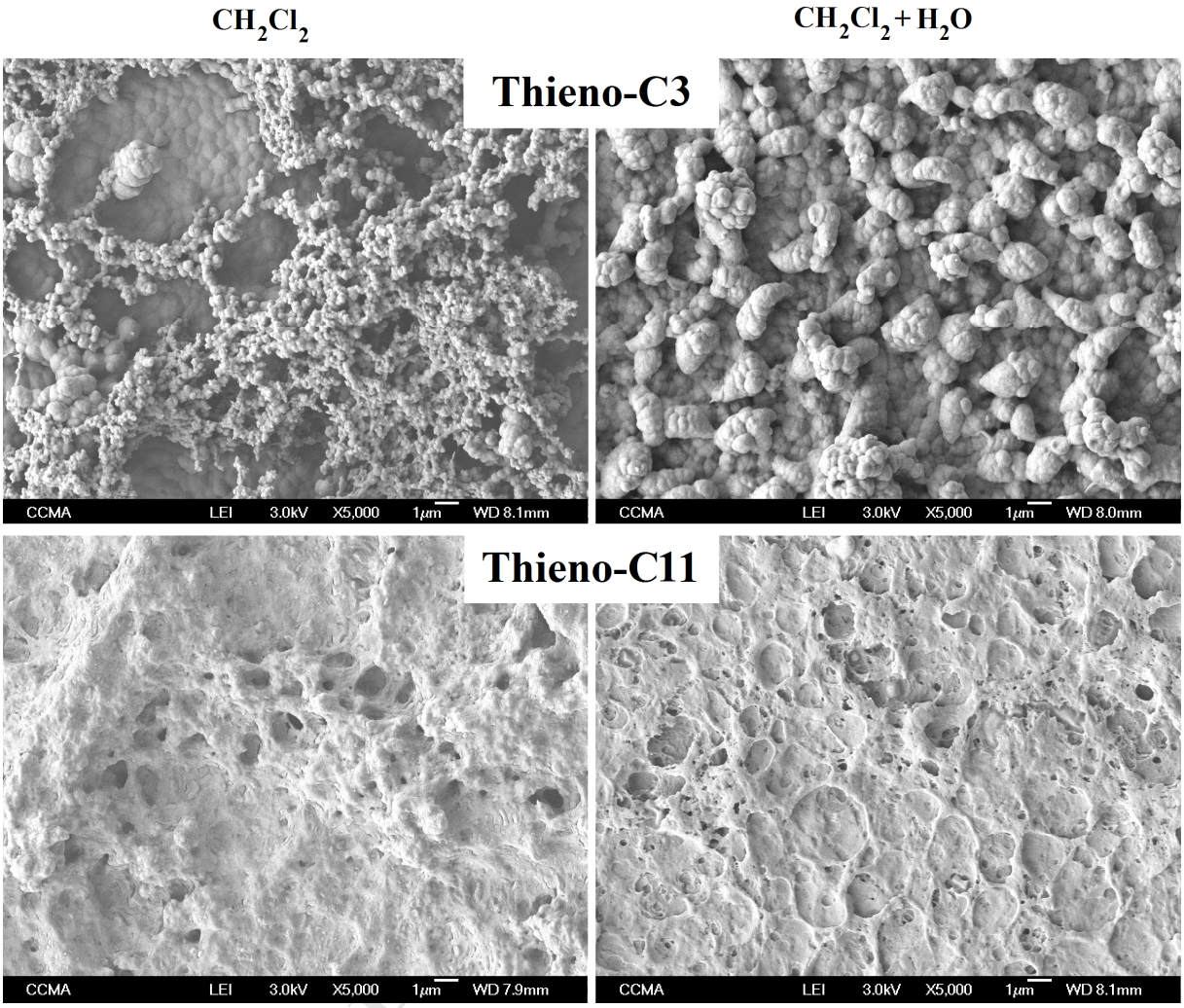

Figure 5. SEM pictures of surfaces obtained from Thieno-C3 and Thieno-C11 and using two different electropolymerization solvents (CH_2Cl_2 and CH_2Cl_2 + H_2O). Number of scans: 3.

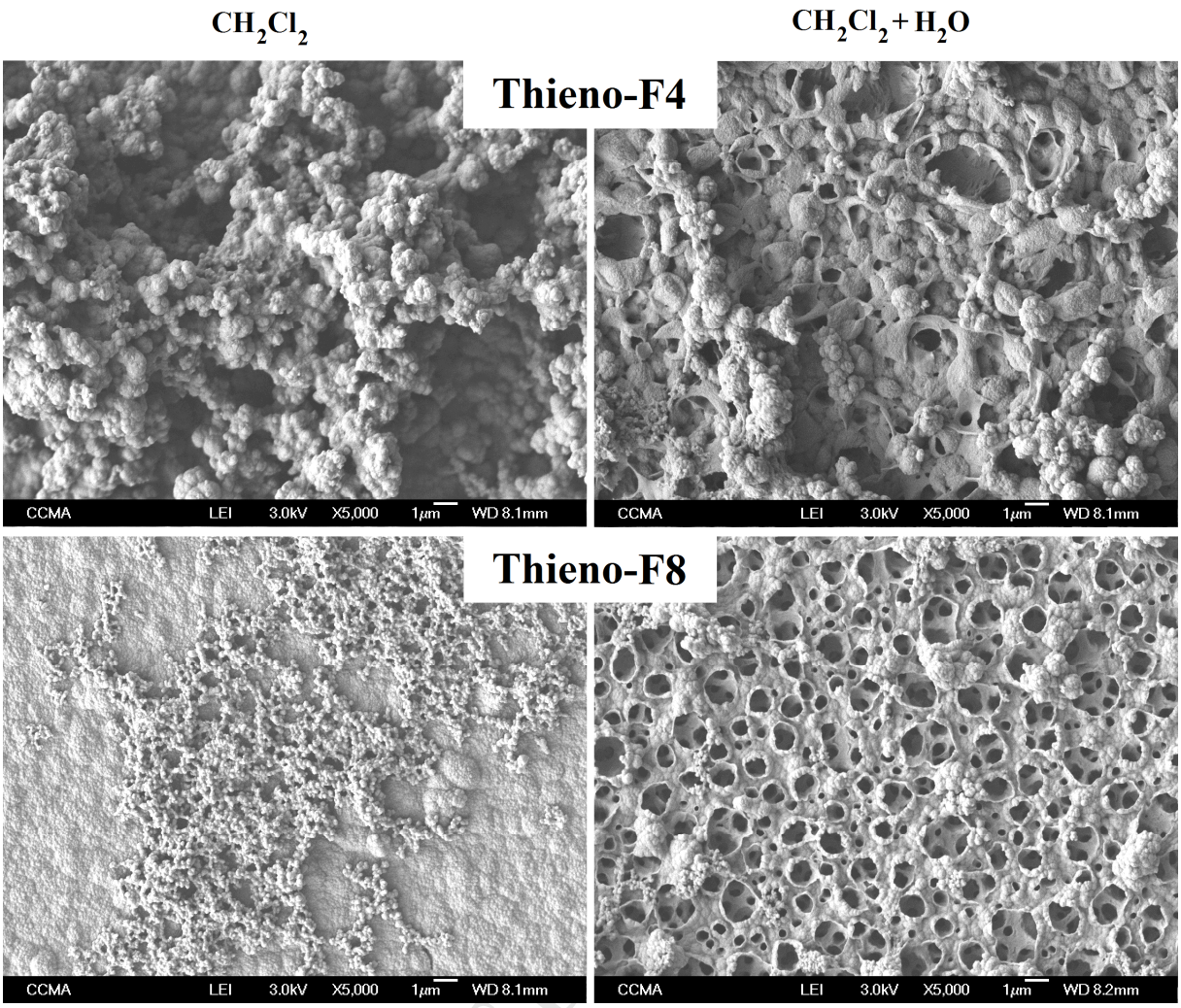

Figure 6. SEM pictures of surfaces obtained from Thieno-F4 and Thieno-F8 and using two different electropolymerization solvents (CH_2Cl_2 and CH_2Cl_2 + H_2O). Number of scans: 3.

Very interesting results are obtained with aromatic groups, confirming the importance of the polymer rigidity (Figure 7). Without H_2O, the polymers are relatively smooth, except Thieno-Pyr. The adding of H_2O leads to a huge amount of hollow spherical structures using Thieno-Fluo, Thieno-Naph and Thieno-BiPh. With Thieno-Ph, the structures are more porous while the trace of very large bubbles are observed with Thieno-diPh.

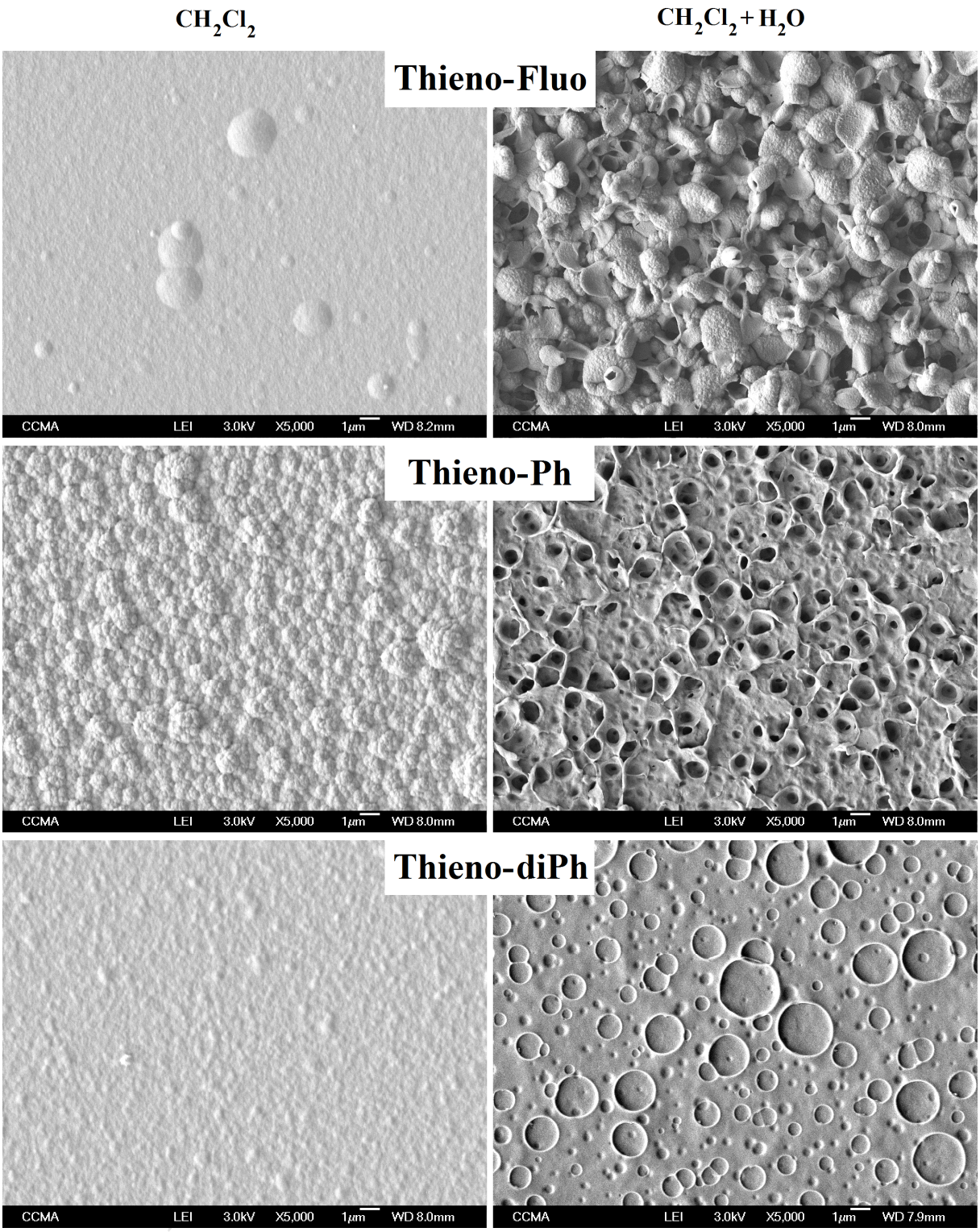

Figure 7. SEM pictures of surfaces obtained from Thieno-Fluo, Thieno-Ph and Thieno-diPh and using two different electropolymerization solvents (CH_2Cl_2 and CH_2Cl_2 + H_2O). Number of scans: 3.

The best results are clearly obtained with Thieno-Pyr (Figure 8 and Figure 9). Here, highly densely packed tree-like structures are observed without H_2O. Moreover, a very huge increase in the size of these tree-like structures is observed with the number of deposition scans. Here, the formation of these very nice structures is probably due to the presence of pyrene units, allowing deposition by π-stacking interactions. Moreover, the fact that the pyrene moiety has an oxidation potential close to that of thieno[3,4-*b*]thiophene may indicate a participation to the polymerization, which is detectable by cyclic voltammetry (a peak at ≈ 0.5-1.0 V *vs* SCE corresponding to pyrene oligomerization is present during the back scans). Indeed, these special results even without adding H_2O were observed only with the pyrene, not the other aromatic substituents. The adding of H_2O leads to an increase of the diameter of the tree-like structures. Moreover, the top of the structures is closed after 1 deposition and becomes open from 3 deposition scans. The presence of very huge open sphere/hemispheres, which look like to corals, is also observed from 3 deposition scans.

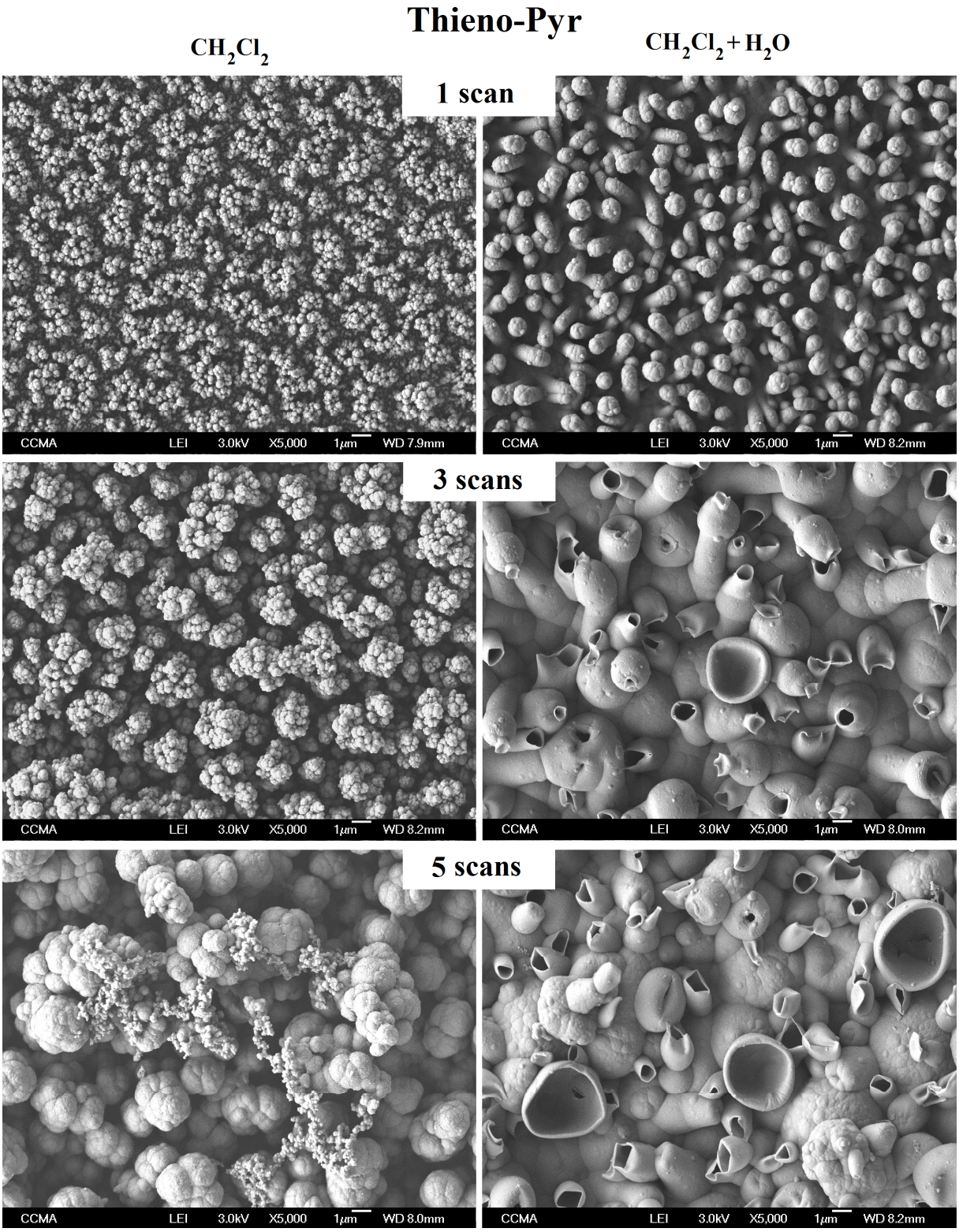

Figure 8. SEM pictures of surfaces obtained from Thieno-Pyr and using two different electropolymerization solvents (CH_2Cl_2 and CH_2Cl_2 + H_2O) and different number of scans (1, 3, 5).

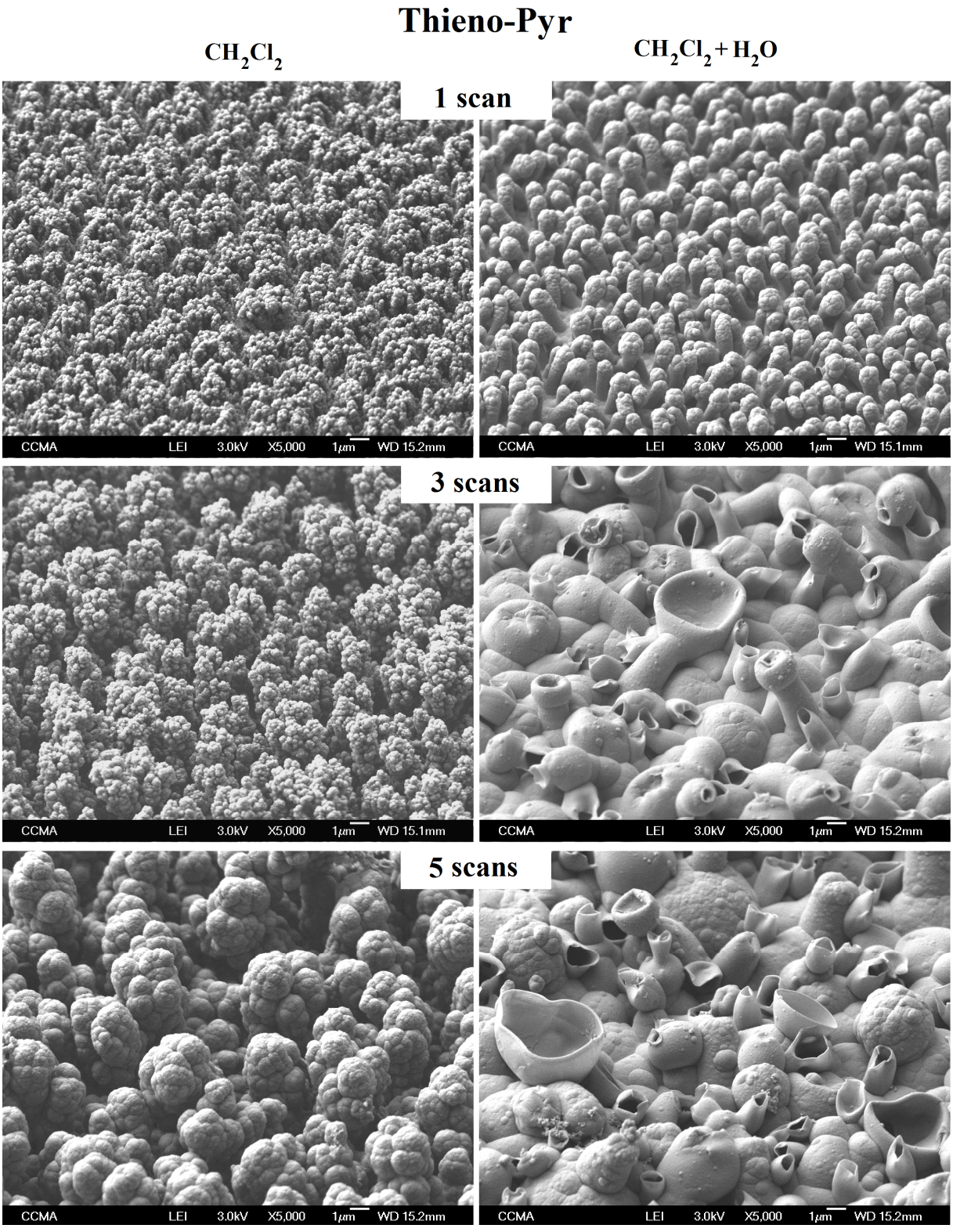

Figure 9. SEM pictures of surfaces obtained from Thieno-Pyr and using two different electropolymerization solvents (CH_2Cl_2 and CH_2Cl_2 + H_2O). The surface inclination for the observation is 45° and different number of scans (1, 3, 5).

The surface wettability of these surfaces was investigated (Table 1). Without H_2O, the contact angles of these surfaces can be very high but after adding H_2O an increase in surface hydrophilicity is almost always observed. As a consequence, the presence of porosity seems to induce here an increase of the wetting properties (Wenzel state) [41]. Indeed, if the polymers are intrinsically hydrophilic such as the polymers with aromatic groups, the presence of surface structures can induce an increase in surface hydrophilicity if the water droplet wets all the surface roughness or an increase in surface hydrophobicity if there is air trapped inside the surface roughness, as described by Cassie-Baxter [11]. For the surfaces obtained with Thieno-BiPh, the increase in surface hydrophobicity can be explained by the fact that the surfaces obtained in CH_2Cl_2 + H_2O (c.f. ESI) is rougher but not significantly porous.

Table 1. Wettability data for the polymers obtained in CH_2Cl_2 and CH_2Cl_2 + H_2O, as electrodeposition solvent.

Monomer	Electrodeposition solvent	θ_w [deg]
Thieno-OH	CH_2Cl_2	114.0 ± 4.0
	CH_2Cl_2 + H_2O	64.0 ± 2.1
Thieno-C3	CH_2Cl_2	118.0 ± 4.2
	CH_2Cl_2 + H_2O	104.6 ± 3.7
Thieno-C5	CH_2Cl_2	109.8 ± 4.6
	CH_2Cl_2 + H_2O	37.1 ± 1.1
Thieno-C7	CH_2Cl_2	132.1 ± 3.6
	CH_2Cl_2 + H_2O	54.7 ± 2.6
Thieno-C9	CH_2Cl_2	130.0 ± 3.2
	CH_2Cl_2 + H_2O	69.0 ± 3.4
Thieno-C11	CH_2Cl_2	117.7 ± 1.2
	CH_2Cl_2 + H_2O	73.2 ± 3.0
Thieno-F4	CH_2Cl_2	140.1 ± 5.0
	CH_2Cl_2 + H_2O	112.6 ± 4.8
Thieno-F6	CH_2Cl_2	138.0 ± 4.2
	CH_2Cl_2 + H_2O	132.8 ± 3.3
Thieno-F8	CH_2Cl_2	136.0 ± 3.7
	CH_2Cl_2 + H_2O	110.1 ± 5.0
Thieno-Ph	CH_2Cl_2	101.5 ± 4.5
	CH_2Cl_2 + H_2O	44.5 ± 1.3
Thieno-BiPh	CH_2Cl_2	86.5 ± 1.6
	CH_2Cl_2 + H_2O	121.2 ± 3.6
Thieno-diPh	CH_2Cl_2	102.4 ± 4.6

	$CH_2Cl_2 + H_2O$	84.3 ± 2.7
Thieno-Naph	CH_2Cl_2	88.2 ± 1.5
	$CH_2Cl_2 + H_2O$	60.7 ± 3.7
Thieno-Fluo	CH_2Cl_2	84.6 ± 1.3
	$CH_2Cl_2 + H_2O$	81.2 ± 3.1
Thieno-Pyr	CH_2Cl_2	131.0 ± 3.5
	$CH_2Cl_2 + H_2O$	55.5 ± 3.3

Absorption and Fluorescence properties of monomers and surfaces

The absorption spectra of Thieno-OH and Thieno-Pyr displayed a peak at about 243 nm (Figure 10). Such maximum is likely to correspond to the absorption of the thiophene core. As Patra A. *et al.*35 once noted: parent thiophene absorbs at λ_{max}=232 nm. The observed 9 nm red-shift (slit size 1.0nm) is due to the presence of a substituent. Thieno-OH shows two narrow bands, with lower absorption. The absorption bands around 266-277 nm and at 293-314 originate from the interaction between the two thiophene rings. The methanol side chain of Thieno-OH shows almost no impact on absorbance (with respect to thienothiophene). With the pyrene chain, the Thieno-Pyr displayed 3 strong bands at 315, 327, 344 nm. These bands are assigned to a single electron $\pi \rightarrow \pi^*$ transition of pyrene rings, containing 3 vibrational sub-bands [19].

Concerning the other studied monomers: the Thieno-Cn with alkyl chains and Thieno-Fn with fluoroalkyl chains displayed similar absorbance spectra compared to Thieno-OH (c.f. ESI). Thus alkyl and fluoroalkyl chains seem to have little influence on electronic excited state levels. Meanwhile the aromatic chains have apparent influences (except for phenyl and diphenyl substituents). Indeed in almost all absorption spectra, spectral contribution of the aromatic moiety is observed [19]. For instance Thieno-Fluo presented bands at 266 nm, 290 nm and 301 nm which correspond to the absorption of the fluorene. Thieno-Naph presented peaks at 265 nm and 275 nm which correspond to the absorbance from the naphthalene (the extinction coefficient are consistent with literature (see Table S1) [42,43].

Emission behavior of monomers are compared to the Thieno-OH. Thieno-OH shows emission maxima at 331 and 414 nm, while the Thieno-Pyr has emission peaks at λ= 375, 395 and 477 nm. The red-shift and broadness shape of the Thieno-Pyr emission at 477 nm might originate from the excimer emission of pyrene which agreed with other previous work in the literature.42 Nevertheless for almost all monomers (except Thieno-Fluo, see Figures in SI), a broad emission band around 470 nm is observed. Moreover all the monomers have an emission band around 330 nm which lies where the Thieno-OH monomer emits. Thus such

emission may arise from thieno[3,4-*b*]thiophene moiety whereas the broad band around 470 nm may come from an excimer. We did not investigate further the absorption and emission properties of the different monomers since we are more interested in the films and surfaces characterizations.

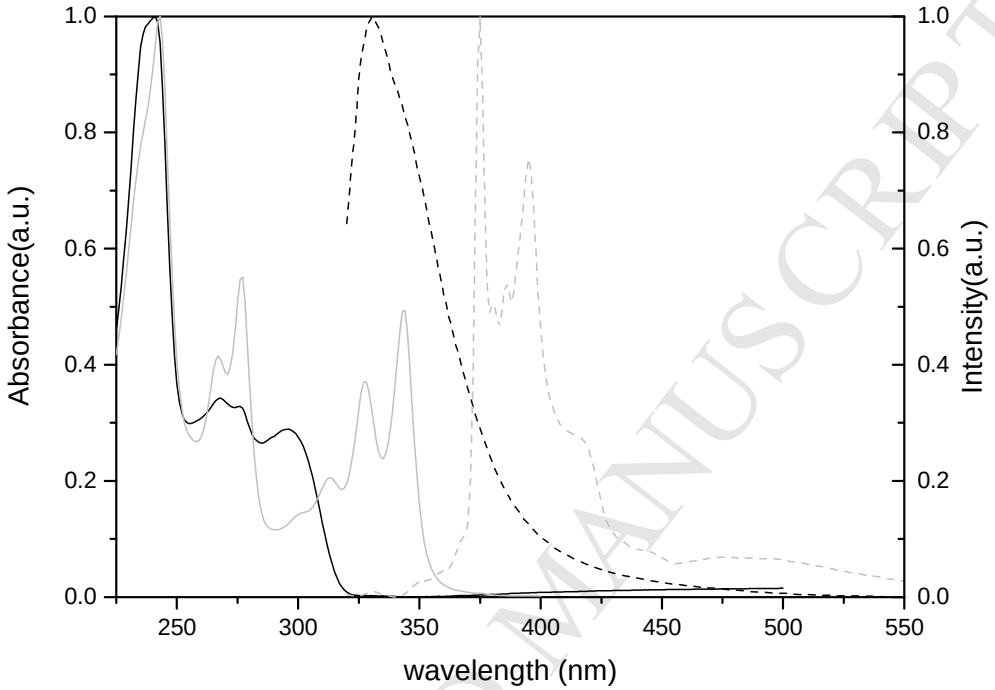

Figure 10. Absorption (solid lines) and emission spectra (dashed lines) for the Thieno-OH (black line) and Thieno-Pyr (grey line) in acetonitrile solution (normalization to 1 at the maximum intensity of each spectrum). Emission spectrum with λ_{EX}=300nm.

Electrodeposition was performed on ITO-glass surfaces with CH_2Cl_2 + H_2O solution in similar conditions as for gold electrode. It was not possible to measure absorption and emission spectra on any ITO films with our steady-state equipment. Indeed, whatever the surface is, it is highly absorbing (dark grey to black color) and highly diffusive. Nevertheless, in some cases we were able to perform fluorescence microscopy imaging in order to compare topography and luminescence signal. Here, we chose to focus only with the polymers obtained with Thieno-OH and Thieno-Pyr. Thieno-OH and Thieno-Pyr are nicely luminescent (Figure 9 and Supp Info). Different substructures can be observed. The fluorescence images correlate well with the SEM images: showing bright spots. In the case of Thieno-Pyr hollow structures are clearly seen and represent ~10% of the 3D-nanostructures. No hollow open spheres could be observed on Thieno-OH surface. The 3D-reconstruction (z-scan on Figure

11) clearly shows a similar thickness of films (less than 5 micrometers) but with different surface coverage. In the case of Thieno-Pyr the density of 3D-substructures is higher than in the case of Thieno-OH. This may arise from the pyrene moiety and π-π interactions between oligomers (Such interactions are not present in Thieno-OH). Using similar illumination, it seems that Thieno-Pyr films are brighter than Thieno-OH, this might come from the pyrene luminescence (or pyrene oligomers luminescence as observed in other works.)

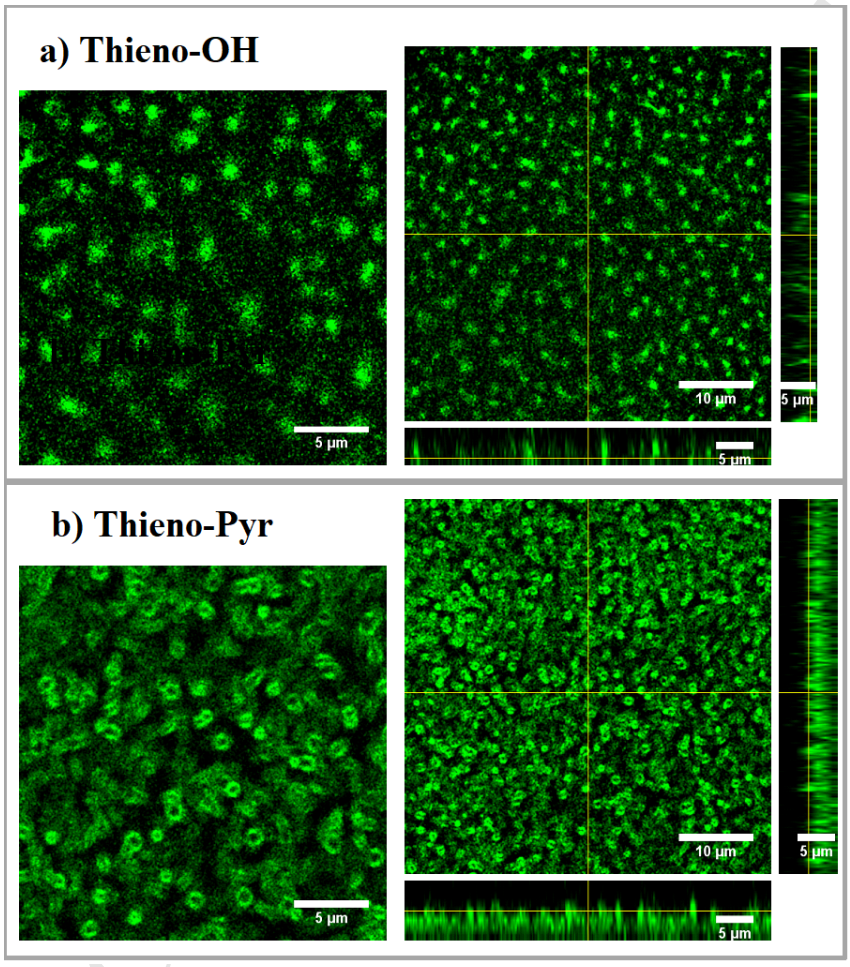

Figure 11. Fluorescence imaging and orthogonal views of a) Poly(Thieno-OH) and b) Poly(Thieno-Pyr) films, (λex: 476 nm λem: 500-640 nm). The surrounding medium is distilled water.

4. Conclusion

We used a templateless electropolymerization in CH_2Cl_2 to control the formation of nanotubular structures. Using thieno[3,4-*b*]thiophene-based monomers, we investigated the

influence of the substituent of various length and nature, as well as the water content in order to release *in-situ* a higher amount of gas bubbles (O_2 and/or H_2). We showed that the pyrene substituent gave exceptional results with the formation of highly densely packed nanotubular structures while the water content highly increased their porosity. As a consequence the surface morphology could change from tree-like to coral-like structure with an increase in surface hydrophilicity. We also observed that both the poly(thieno[3,4-b]thiophene) polymers and the substituents are fluorescent while the nanostructures seemed to amplify their intensity.

5. Acknowledgment

The authors thank Alyssia Mari from the Centre Commun de Microscopie Appliquée (CCMA, Université Nice Sophia Antipolis) for the preparation of the substrates for the SEM analyses.

References

[1] Z. Cheng, J. Gao, L. Jiang, Langmuir 26 (2010) 8233–8238.

[2] S. Sandoval, E. Pach, B. Ballesteros, G. Tobias, Carbon 123 (2017) 129–134.

[3] R. Majidi, H.R. Taghiyari, O. Ori, Nanotubes Carbon Nanostruct. 25 (2017) 646–651.

[4] L. Wu, C. Man, H. Wang, X. Lu, Q. Ma, Y. Cai, W. Ma, Pharm. Res. 30 (2013) 412–423.

[5] S.G. Balasubramani, D. Singh, R.S. Swathi, J. Chem. Phys. 141 (2014) 184304.

[6] M. Martincic, G. Tobias, Exp. Opin. Drug Delivery 12 (2015) 563–581.

[7] C.J. Shearer, A. Cherevan, D. Eder, Adv. Mater. 26 (2014) 2295–2318.

[8] K.K.S. Lau, J. Bico, K.B.K. Teo, M. Chhowalla, G.A.J. Amaratunga, W.I. Milne, G.H. McKinley, K.K. Gleason, Nano Lett. 3 (2003) 1701–1705.

[9] K.K. Jung, Y. Jung, C.J. Choi, J.S. Ko, ACS Omega 3 (2018) 12956–12966.

[10] D.J. Babu, M. Mail, W. Barthlott, J.J. Schneider, Adv. Mater. Interfaces 4 (2017) 1700273.

[11] A.B.D. Cassie, S. Baxter, Trans. Faraday Soc. 40 (1944) 546–551.

[12] A. Marmur, Langmuir 20 (2004) 3517–3519.

[13] A. Marmur, Langmuir 24 (2008) 7573–7579.

[14] A. Marmur, Langmuir 19 (2003) 8343–8348.

[15] H.□A. Lin, S.□C. Luo, B. Zhu, C. Chen, Y. Yamashita, H.□h. Yu, Adv. Funct. Mater. 23 (2013) 3212–3219.

[16] M. Paulose, H.E. Prakasam, O.K. Varghese, L. Peng, K.C. Popat, G.K. Mor, T.A. Desai, C.A. Grimes, J. Phys. Chem. C 111 (2007) 14992–14997.

[17] Y.-K. Lai, Y.-X. Tang, J.-Y. Huang, F. Pan, Z. Chen, K.-Q. Zhang, H. Fuchs, L.-F. Chi, Sci. Rep. 3 (2013) 3009.

[18] L. Qu L, G. Shi, F. Chen, J. Zhang, Macromolecules 36 (2003) 1063−1067.

[19] G. Lu, G. Shi, J. Electroanal. Chem. 586 (2006) 154–160.

[20] J. Yuan, L. Qu, D. Zhang, G. Shi, Chem. Commun. 0 (2004) 994−995.

[21] J.T. Kim, S.K. Seol, J.H. Je, Y. Hwu, G. Margaritondo, Appl. Phys. Lett. 94 (2009) 034103.

[22] C. Debiemme-Chouvy, A. Fakhry, F. Pillier, Electrochim. Acta 268 (2018) 66–72.

[23] C. Debiemme-Chouvy, Electrochem. Solid-State Lett. 10 (2007) E24−E26.

[24] A. Fakhry, H. Cachet, C. Debiemme-Chouvy, Electrochim. Acta 179 (2015) 297−303.

[25] A. Fakhry, F. Pillier, C. Debiemme-Chouvy, J. Mater. Chem. A 2 (2014) 9859−9865.

[26] C. Debiemme-Chouvy, Electrochem. Commun. 11 (2009) 298-301.

[27] B. Parakhonskiy, D. Shchukin, Langmuir 31 (2015) 9214−9218.

[28] B. Parakhonskiy, D. Andreeva, H. Möhwald, D.G. Shchukin, Langmuir 25 (2009) 4780−4786.

[29] T. Darmanin, F. Guittard, J. Mater. Chem. A 4 (2016) 3197–3203.

[30] C.R. Szczepanski, I. M'Jid, T. Darmanin, G. Godeau, F. Guittard, J. Mater. Chem. A 4 (2016) 17308–17323.

[31] T. Darmanin, G. Godeau, F. Guittard, E.L. Klimareva, I. Schewtschenko, I.F. Perepichka, ChemNanoMat 4 (2018) 656–662.

[32] A. Gbilimou, T. Darmanin, G. Godeau, F. Guittard, ChemNanoMat 4 (2018) 140–147.

[33] S. Bai, Q. Hu, Q. Zeng, M. Wang, L. Wang, ACS Appl. Mater. Interfaces 10 (2018) 11319–11327.

[34] G. Ramos Chagas, T. Darmanin, G. Godeau, F. Guittard, Electrochim. Acta 269 (2018) 462–478.

[35] G. Ramos Chagas, F. Guittard, T. Darmanin, ACS Appl. Mater. Interfaces 8 (2016) 22732–22743.

[36] G. Ramos Chagas, R. Akbari, G. Godeau, M. Mohammadizadeh, F. Guittard, T. Darmanin, ChemPlusChem 82 (2017) 1351–1358.

[37] A. Patra, Y.H. Wijsboom, G. Leitus, Chem. Mater. 23 (2011) 896-906.

[38] G. Buemi, Bull. Chem. Soc. Jpn. 62 (1989) 1262–1268.

[39] Y. Wada, Y. Asada, T. Ikai, K. Maeda, T. Kuwabara, K. Takahashi, S. Kanoh, ChemistrySelect 1 (2016) 703–709.

[40] V.S. Saji, K.K. Zong, M. Pyo, J. Photochem. Photobiol. A: Chem. 212 (2010) 81–87.

[41] R.N. Wenzel, Ind. Eng. Chem. 28 (1936) 988–994.

[42] I.B. Berlman, Handbook of fluorescence spectra of aromatic molecules, Academic press new York and London, 1965.

[43] H. Wynberg, D.J. Zwanenburg, Tetrahedr. Lett. 8 (1967) 761–764.

[44] J. Jang, J.H. Oh, Adv. Mater. 15 (2003) 977–980.

Graphical Abstract